1	Title: Inputs of root-derived carbon into soil and its losses are associated with pore-size			
2	distributions			
3				
4	M. Y. Quigley <sup>1</sup> * and A.N. Kravchenko <sup>2</sup>			
5	<sup>1</sup> Department of Horticulture, Michigan State University, East Lansing MI 48824			
6	<sup>2</sup> Department of Plant, Soil and Microbial Sciences, Michigan State University, East Lansing MI			
7	48824			
8				
9	*Corresponding author:			
10	Email: quigle30@msu.edu			
11	Mail: 1066 Bogue St. A288			
12	East Lansing, MI 48824			
13	Phone: (01) 517-355-5191			
14				
15				
16	<b>Keywords:</b> X-ray computed micro-tomography, root exclusion, soil incubation, cereal rye, <sup>13</sup> C			
17	pulse labeling, cover crop			
18				
19	Abbreviations:			
20	μCT – X-ray computed micro-tomography			
21				

23

24

25

26

27

28

29

30

31

32

33

34

35

36

37

38

39

40

41

42

43

#### **ABSTRACT**

Placement and fate of photo-assimilated carbon (C) newly added to the soil are important contributors of soil health. Soil pores control the movement of gasses, water, and microorganisms, thus potentially influencing new photo-assimilated C gains and losses. The objective of this study was to explore the associations between soil pores and additions and losses of root-derived C. Young cereal rye (Secale cereale L.) plants were grown in the soil with inherent pore architecture destroyed by sieving and in the soil with the intact pore architecture, with each rye planted container having a section inaccessible to plant roots. Plants were pulse labeled with <sup>13</sup>CO<sub>2</sub>, followed by sampling for intact soil cores and subjecting them to X-ray computed micro-tomography (µCT) scanning, some immediately after collection and some after a 21-day incubation. From the scanned cores we obtained soil micro-samples in specific locations corresponding to  $\mu CT$  images. The  $\mu CT$  images were used to quantify pore size distributions of the micro-sample soils, while soil  $\delta^{13}$ C signatures provided a quantitative measure of the presence of root-derived C before and after the incubation. In the intact soils,  $\delta^{13}$ C was positively associated with >90 µm Ø pores, likely reflecting preferential rye root growth into legacy root channels. In soils with existing pore architecture destroyed, <sup>13</sup>C was preferentially added to 15-90  $\mu$ m Ø pores when the soil was accessible to roots and to 7-40  $\mu$ m Ø pores when the soil was accessible only to fungi, yet after the incubation the associations between <sup>13</sup>C and pores were lost. The results identified the pore sizes associated with rootderived C additions to the soil via root and fungal routes and highlighted the importance of inherent pore architecture on the placement and persistence of such additions.

#### 1. INTRODUCTION

45

46

47

48

49

50

51

52

53

54

55

56

57

58

59

60

61

62

63

64

65

66

67

Soils play a major role in global carbon (C) cycling, storing almost twice the amount of C present in the atmosphere (Davidson and Janssens, 2006; Falkowski et al, 2000; Lal, 1999; Swift, 2001). Agricultural soils have a large untapped C storage capacity that can contribute to climate change mitigation (Dungait et al, 2012; Kell, 2012; Lal, 2011; Oechel and Vourlitis, 1994). Soil organic C is also strongly linked to soil fertility and crop yields, thus making the task of increasing its storage in agricultural soils important to both agricultural sustainability and soil health (Bauer and Black, 1994; Lal, 2006; Melsted, 1954). Agricultural management can greatly influence soil C gains and losses (Senthilkumar et al, 2009; Syswerda et al, 2011). Conventionally tilled and fertilized agricultural systems are often associated with C losses (Abraha et al, 2018; Grandy and Robertson, 2007; Ruan and Robertson, 2013). Including cover crops in the rotation, i.e. planting of a non-cash crop between cash crops, can provide erosion control, suppress weeds, increase water holding capacity and fertility, as well as enable soil C gains; although the gains can take years to be reliably detected (Necpálová et al, 2014; Rorick and Kladivko, 2017). The mechanisms enabling C gains in agricultural systems with cover crops are not fully understood (Austin et al, 2017). For example, increasing plant biomass inputs is believed to be one of the best ways to improve soil C (Paustian et al, 2016). However, crops producing large amounts of biomass do not always lead to substantial C gains (Chimento et al, 2016; Garten and Wullschleger, 1999; Sprunger and Robertson, 2018), indicating that not only the amount of C input, but its subsequent protection within the soil is required for increasing sequestration.

Protection of soil C is driven by its accessibility to microbial decomposers and by environmental conditions within the soil matrix beneficial for microbial functioning and

decomposition. Soil matrix consists of an infinity of diverse microenvironments differing in their water and oxygen regimes, gas flows, and nutrient influxes. Characteristics and properties of soil microenvironments are largely defined by soil pores that control the fluxes of water and gases, microbial access to C sources, as well as microorganism movement and nutrient transport (Ekschmitt et al, 2005, 2008; Kravchenko and Guber, 2017; Park et al, 2007; Rabot et al, 2018; Young et al, 2001). While links between pores of specific size ranges and soil C losses or protection have been established (Ananyeva et al, 2013; Bailey et al, 2017; Quigley et al, 2018; Strong et al, 2004), the processes behind these associations have yet to be elucidated.

Plants modulate the links between soil C protection and pore characteristics in a multitude of ways. First, they provide spatially variable inputs of photo-assimilated C belowground via dead root biomass and rhizodeposits from live roots (Bais et al., 2006; Badri et al., 2009). The exact location of where the new organic input is placed can affect whether it will remain in the soil protected from decomposition or be immediately consumed by microorganisms. Second, roots affect pore architecture in their immediate vicinity, i.e., in the rhizosphere (Carminati et al., 2010; Koebernick et al., 2017; Benard et al., 2019; Koebernick et al., 2019; Lucas et al., 2019; Zhang et al., 2020) as well as in the entire soil matrix (Dexter, 1987; Graecen et al 1968). Third, presence of actively growing roots is known to stimulate enhanced decomposition of inherent soil organic matter in a process known as rhizosphere priming (Kuzyakov, 2002; Pausch et al., 2013). The relationships between roots and pores are reciprocal as pore size distributions also affect root growth (Bengough et al, 2006; Bowen, 1981).

Previous studies have shown that roots, as compared to shoots, contribute a disproportionate amount (up to 75%) of C into the soil (Austin et al, 2017; Gale et al, 2000; Kong and Six, 2010; Mazzilli et al, 2015; Rasse et al, 2005). This contribution can be in a form

of actual root biomass or through root exudates and rhizodeposits. Around 30-50% of belowground biomass can be derived from rhizodeposition (Barber and Martin, 1976; Kuzyakov et al, 2003; Meharg and Killham, 1991). Root exudates consist of organic acids, amino acids, and other small, highly soluble and easy to decompose compounds, although mucilage and other harder to decompose materials can also be produced (Brimecombe et al, 2011; Dungait et al, 2012). The easily decomposable compounds can be quickly taken up by soil microbes, adding to microbial biomass. Up to 25-30% of microbial biomass C can be derived from actively growing plants (Austin et al, 2017; Williams et al, 2006). Processing of C by soil microorganisms is one of the first steps in soil organic matter production. The processed C can attach to mineral particles, where it then remains, protected from further degradation (Grandy and Neff, 2008; Jackson et al, 2017; Kallenbach et al, 2015, 2016; Wieder et al, 2014). Therefore, spatial patterns in the distribution of roots and their exudates can play an important role in soil C inputs and protection.

Soil structure and pore architecture strongly depend on agricultural management. Intensive tillage has been associated with an increased presence of 40-90 µm pores (Wang et al, 2012), which has also been linked with C losses (Ananeyeva et al, 2013), especially the losses of newer C (Quigley et al, 2018). Pores of this size range are created through either mechanical wetting/drying and freeze/thaw cycles or by smaller plant roots or microfauna. On the other hand, management with continuous presence of live vegetation cover, e.g., cover crops, has been related to a higher presence of >90 µm pores and higher total porosity, which are associated with larger roots (Kravchenko et al, 2014). Pores of size 6.5-40 µm have been associated with carbon storage, potentially from anaerobic conditions that exist due to water filling of these pore under most field conditions. Keiluweit et al. (2017) observed decomposition rates 10 times slower

under anaerobic conditions in upland soils. Carbon addition and losses can be decoupled from pore structure due to legacy root channels (Quigley et al, 2018). Roots tend to grow in old established root channels (Rasse and Smucker, 1998), which can affect the storage and protection of soil carbon. Roots creating new pores are in direct contact with the soil, which may lead to carbon losses as paths to reach smaller pores where C storage takes place might be blocked (Quigley et al, 2018). On the other hand, roots tend to grow in larger pores due to ease of growth, which may lead to more C protection as root exudates can more easily be transported to smaller pores where carbon storage is thought to occur.

The main goal of the study was to evaluate the influence of pores on localization of newly added root-derived C and its subsequent losses. The first objective was to identify the relationships between soil pores and the new C added to soil by growing roots. The second objective was to determine if the newly added plant-derived C was lost during subsequent incubation and how the losses were associated with pores of different sizes.

### 2 MATERIALS AND METHODS

Cereal rye (*Secale cereale* L.), a common cover crop in the Midwestern US, was used in the greenhouse experiment of this study. Two soil treatments were explored, one with the original soil structure intact and one where soil structure was destroyed by sieving through a 1-mm sieve. Destroying the structure eliminated the existing pore architecture, allowing for the effects of newly grown rye roots on soil pore formation and C protection to be separated from legacy effects and to be more easily detected. After 3 months of rye growth, intact soil samples collected from the containers were subjected to X-ray computed micro-tomography (μCT) allowing us to explore formation and properties of soil pores. Rye plants were enriched with <sup>13</sup>C

via pulse labeling, which enabled tracking newly added root-derived C and exploring its associations with soil pores. A rough outline of the experimental design can be found in Fig. 1.

#### 2.1 Soil collection

Soil for the greenhouse experiment was collected from Long Term Ecological Research site established in 1989 at Kellogg Biological Station, Hickory Corners, MI (42°24′N, 85°24′W). The soil is a fine-loamy, mixed mesic Typic Hapludalf of the Oshtemo and Kalamazoo series developed on glacial outwash with an intermixed loess layer (Crum and Collins, 1995; Luehmann et al, 2016). Soil for the experiment was collected in May of 2016 from long-term (since 1989) chisel-plowed agricultural experimental plots in corn-soybean-wheat rotation during the wheat phase of the rotation. Soil was collected between wheat rows at 0-10 cm depth.

Two soil structure treatments were created. In the first treatment, referred further on as intact-structure soil, 8 cm of soil was taken using large spades with minimal disturbance and placed into 30 x 21 cm size containers as a relatively intact layer. In the second treatment, referred further on as destroyed-structure soil, the soil was sieved through a 1 mm sieve to destroy the existing soil structure and specifically previous root channels. The sieved soil was also placed into 30 x 21 cm containers to an 8 cm depth and packed as necessary to achieve  $\sim$ 1.4 g cm<sup>-3</sup> density, consistent with the average density of the intact-structure containers. Packing was done by calculating the weight of soil needed to achieve  $\sim$ 1.4 g cm<sup>-3</sup> (7,056 g) and making sure that the soil height was 8 cm and adjusting via shaking the container. There were four replicated containers in each soil structure treatment, for a total of 8 containers. Each container had a circular enclosure at one end to create a zone free of the immediate influence of plant roots. The

enclosures were made of 35 µm size mesh and were 6 cm in diameter. The soil within enclosures was inaccessible to plant roots but was accessible to fungal hyphae.

Rye seeds were hand planted at 3 cm depth and at 4 cm distances from each other outside of the no-root enclosures with 9 rye plants per container. Rye was grown in the greenhouse under optimized watering and light conditions for plant growth (maintained between field capacity and wilting point and 12 hour light conditions) for a total of three months. Lighting was preprogrammed, while watering was done as necessary depending on conditions in the greenhouse (more often on hotter days, less often on cooler days).

Additionally, 4 control containers, two per each soil structure treatment, were filled with soil as described above, but not planted. These containers were kept in the greenhouse next to the planted containers for the entire period of rye growth and were watered on a regular basis along with planted containers.

## 2.2 Pulse labeling

Pulse labeling began two weeks after rye establishment and was repeated every 10 days until the end of the three-month growth period for a total of 8 labeling events. At each labeling event, the rye containers were moved into a plexiglass chamber. One gram of 99% <sup>13</sup>C enriched CaCO<sub>3</sub> was placed in the chamber. The chamber was then sealed with duct tape to create an airtight enclosure. Then 1M H<sub>2</sub>SO<sub>4</sub> was added to CaCO<sub>3</sub> in excess via syringe. The evolved CO<sub>2</sub> was estimated to generate approximately 10% atm enrichment in the chamber. The chamber was equipped with a fan to evenly circulate the evolved CO<sub>2</sub>. Plants were labeled for 24 hours (Bird et al, 2003; Toosi et al, 2017) and then removed from the plexiglass chamber until the next labeling event. The control containers were not subjected to pulse labeling and were used to determine <sup>13</sup>C natural abundance.

## 2.3 Sample collection

At the end of the three-month rye growth period, four intact cores (8 mm Ø and  $\sim$ 2 cm height) were taken from each container, two cores from the root exclusion zone and two cores adjacent to rye plants. The cores were taken at 0-5 cm depth using a beveled 3 mL Luer-Lok polypropylene syringe (BD, Franklin Lakes NJ, USA) and air-dried. Two additional cores (8 mm Ø and  $\sim$ 2 cm) per container were taken to calculate bulk density.

Roots were collected from the remaining soil and air-dried, then analyzed for  $\delta^{13}C$  to determine the enrichment of the rye plants in each container. Roots from each box were washed of soil and 5 roots were randomly collected per box for a total of 40 root samples. In addition, three replicate composite samples comprising roots from all 8 boxes were analyzed, resulting in a total of 43 samples for root isotope analyses.

All cores were X-ray  $\mu$ CT scanned (see 2.4). After that, half of the cores were subjected to destructive micro-sampling for  $\delta^{13}$ C analysis. The samples collected from these cores are referred to as Pre-incubation samples. The remaining cores were incubated for 21 days (see 2.5), scanned again, and then also subjected to micro-scale sampling for  $\delta^{13}$ C. These samples are referred to as Post-incubation samples.

Micro-scale sampling was conducted using a custom-made soil sampling device (Fig. 2), which facilitated matching of the  $\delta^{13}$ C data with  $\mu$ CT images. The device consisted of five 2 mm Ø and 5 mm deep open metal rods and had an etched vertical mark on its side to align with the etched mark on the side of the cores. The marks on the cores were visible on the  $\mu$ CT scans and thus it was possible to match the  $\delta^{13}$ C data collected via micro-sampling device with the soil core's image information. The sampling proceeded as following: first, soil was gently pushed out

of the core into a plastic cylinder (8 mm  $\varnothing$  and 2 mm height). Once the top 2 mm of the soil were within the cylinder it was evenly cut off using a razor blade at the bottom of the cylinder. This topsoil layer was then discarded. Then, the main layer of the soil, 5 mm in height, was similarly procured from the core into a separate marked cylinder, with the mark on the cylinder aligned with the etched mark on the core. The cylinder was aligned with the micro-sampling device, which was pushed into the soil filling all 5 open rods with the soil. Set positions of the rods within the sampling device ensured convenient and accurate tracing of the locations of the specific samples to the 3D images of the soil core. Approximately 10-20  $\mu$ g of soil was collected into each rod for  $\delta^{13}$ C analysis.

## 2.4 Collection of µCT images

The air-dried cores were scanned on the bending magnet beam line, station 13-BM-D of the GeoSoilEnvironCARS at the Advanced Photon Source, Argonne National Laboratory, IL.

Images were collected with the Si (111) double crystal monochromator tuned to 28 keV incident energy, the distance from sample to source was approximately 55 m, and the X-ray dose is estimated to be 1 kGy. Two-dimensional projections were taken at 0.25° rotation angle steps with a one second exposure and combined into a three-dimensional image consisting of 1198 slices with 1920 by 1920 pixels per slice for Pre-incubation cores. Scan time was ~20 minutes.

This resulted in a voxel size of 4.2 μm. Scans of Post-incubation cores had 1200 slices of 1920 by 1920 pixels and resulted in a voxel size of 4.3 μm. The data were pre-processed by correcting for dark current and flat field and reconstructed using the GridRec fast Fourier transform reconstruction algorithm (Rivers, 2012).

The indicator kriging method was utilized for segmentation of pore/solid in the images using 3DMA-Rock software (Oh and Lindquist, 1999; Wang et al, 2011). Total image porosity

(pores > 7  $\mu$ m Ø) and the size distribution of > 7  $\mu$ m Ø pores were obtained from each core. The smallest identified pores were 7  $\mu$ m, which is ~1.5 times the voxel size. Pores smaller than 7  $\mu$ m may rarely have been identified down to 5  $\mu$ m due to partial volume effects.. The total image porosity was calculated as the percent of pore voxels in the total number of voxels in the image. Pore size distribution was obtained using the burn number distribution approach as implemented in 3DMA-Rock (Ananyeva et al, 2013; Lindquist et al, 2000). Briefly, the burn number represents the shortest distance from the pore medial axis to the pore wall. For clarity, burn numbers have been converted into pore diameters. Reported pore size distributions are for the subsamples, but the pore size distributions for the entire images can be found in Supplemental Fig. 1, 2. We specifically focused the data analyses on the pores of the following four diameter ranges: 7-15  $\mu$ m, 15-40  $\mu$ m, 40-90  $\mu$ m, and >90  $\mu$ m. These sizes were chosen to match size ranges used in previous analyses of the studied soil that have demonstrated strong associations with C (Ananyeva et al, 2013; Kravchenko et al, 2014, 2015; Quigley et al, 2018; Wang et al, 2012, 2013). Sample CT images can be found in Fig. 3.

### 2.5 Incubation experimental design

Prior to incubation, water was added from the top of the cores to achieve 50% of water filled pore space. The cores were sealed at the bottom and placed into 10 ml vacutainers (BD Franklin Lakes NJ, USA) with 1 mL of de-ionized water added to the bottom to maintain high humidity and consistent moisture levels. Samples were then incubated at 22.4±0.1°C for 21 days.

Gas samples for total CO<sub>2</sub> and <sup>13</sup>CO<sub>2</sub> measurements were taken at day 1, 3, 7, 14, and 21. In order to have enough gas to sample at each sampling time, containers were over pressurized when purged with CO<sub>2</sub> free air at the start of the incubation and after every sampling. At each

sampling time, 1 mL of headspace was collected via syringe for  $CO_2$  concentration. For  $\delta^{13}C$  measurements, 3 mL of headspace gas was sampled via syringe and then 9 mL of  $CO_2$  free compressed air was used to fill the 12 mL sample vials to near atmospheric pressure. All  $CO_2$  free compressed air used was measured for both  $CO_2$  concentration and  $\delta^{13}C$ . After each gas sampling, the headspace was flushed using  $CO_2$  free air.

## 2.6 Gas and soil C and $\delta^{13}$ C analyses

A LI-820 CO<sub>2</sub> infrared gas analyzer (Lincoln, Nebraska, USA) was used to take CO<sub>2</sub> concentration measurements. The  $\delta^{13}$ C and total C analyses of soil and plant samples were conducted at the Stable Isotope Facility at the University of California Davis. Soil samples were analyzed using an Elementar Vario EL Cube or Micro Cube elemental analyzer (Elementar Analysensysteme GmbH, Hanau, Germany) interfaced to a PDZ Europa 20-20 isotope ratio mass spectrometer (Sercon Ltd., Cheshire, UK). Plant samples were analyzed using a PDZ Europa ANCA-GSL elemental analyzer interfaced to a PDZ Europa 20-20 isotope ratio mass spectrometer (Sercon Ltd., Cheshire, UK). Gas samples were analyzed using a ThermoScientific GasBench system interfaced to a ThermoScientific Delta V Plus isotope ratio mass spectrometer (ThermoScientific, Bremen, Germany).

The C isotopes are reported relative to Vienna PeeDee Belemnite with a 0.1‰ standard deviation for all samples.

## 2.7 Statistical analysis

Analysis of the studied experimental factors was conducted using the mixed model approach via PROC MIXED procedure of SAS (Version 9.4, SAS Inc., 2009). The statistical

model for analysis of  $CO_2$  and  $\delta^{13}CO_2$  data collected during incubation included fixed effects of soil structure (destroyed vs. intact), root presence (root accessible vs. inaccessible), day (1, 3, 7, 14, and 21), and their interactions. The model also included the random effects of containers nested within soil structure and root presence by container interaction. Day was treated as a repeated measure factor following the approach described by Milliken and Johnson (2009).

The statistical model for analysis of the soil data, including pore volumes, total C, and  $\delta^{13}$ C, consisted of the fixed effects of the soil structure, root presence, incubation status (Pre vs. Post), and their interactions. The model included the random effect of containers nested within soil structure as well as the interaction of root presence with container.

The normality assumption was visually assessed using normal probability plots and stemand-leaf plots, while equal variance assumption was assessed using Levene's test. Where the equal variance assumption was violated, analysis with unequal variances was conducted (Milliken and Johnson, 2009). The differences among the treatments are reported as statistically significant at  $\alpha$ =0.05.

Correlation and simple linear regression analyses between pore characteristics and  $CO_2$ , soil  $\delta^{13}C$  and  $CO_2$   $\delta^{13}C$  signatures were conducted using PROC CORR and PROC REG procedures of SAS.

#### 3. RESULTS

## 3.1 Soil and plant characteristics

Soils with destroyed and intact structure did not differ from each other in terms of basic soil characteristics, including bulk density, soil organic C, and total nitrogen (N) (Table 1).

Plants performed somewhat better in the destroyed structure soil producing numerically, but not statistically significant, higher root biomass and aboveground biomass.

Labeling successfully enriched rye plants. The average  $\delta^{13}C$  signature in the roots was equal to 546 ‰ with very similar  $\delta^{13}C$  values observed in the containers from both soil structures (Table 1).

## 3.2 Pore characteristics

The image-based porosity (pores >7  $\mu$ m Ø) ranged from 19 to 32% (Fig. 4). Overall, the image-based porosity significantly increased after incubation (p<0.05, Fig. 4); and was numerically higher, but not statistically significant, in the soil with destroyed than with intact structure. The increase after the incubation was most pronounced in the destroyed structure soil (Fig. 4).

As expected, destroying soil structure by sieving modified soil pore-size distributions (Supplemental Table 1). It led to a greater abundance of 15-40  $\mu$ m Ø pores and fewer >90  $\mu$ m Ø pores (Fig. 5a and 5d). Incubation increased the abundance of the 7-15  $\mu$ m Ø pores (Fig. 5a). The effect of the incubation on 7-15  $\mu$ m Ø pores was stronger in the soil with destroyed structure with roots. Prior to incubation 7-15  $\mu$ m Ø pores were more abundant in the soil not exposed to plant roots than in the soil exposed to roots, however, after incubation the difference disappeared. Exposure to roots did not affect pores of any other sizes.

## 3.3 Photo-assimilated C

As expected, high  $\delta^{13}$ C signatures were observed in the soil exposed to plant growth (Fig. 6). However, some enrichment was observed in the soil from no-root enclosures as well. After

21-day incubation soil  $\delta^{13}$ C signatures dropped substantially and in the soil from no-root enclosures they became non-distinguishable from the control levels.

While no statistically significant differences were observed,  $CO_2$  emissions during incubation were numerically higher in the soil exposed to root growth than in the soil not exposed to roots (Supplemental Fig. 3a). The  $\delta^{13}C$  signatures of the  $CO_2$  emitted from the root-exposed soil were also numerically higher, but not statistically significant, than those from the soil not exposed to roots (Supplemental Fig. 3b). The  $\delta^{13}C$  signatures of emitted  $CO_2$  decreased with incubation time in both root-exposed and not exposed soil.

## 3.4 Associations between pores and $\delta^{13}$ C signatures of soil and CO<sub>2</sub>

Prior to incubation  $\delta^{13}$ C signatures in the soil with destroyed structure were significantly positively correlated with 15-40  $\mu$ m and 40-90  $\mu$ m  $\varnothing$  pores in the soil exposed to plant roots, while no correlations with pores of any size were observed after the incubation. Scatter plots of the data and simple linear regression lines fitted to the data are reported on Fig. 7, while summary of correlation coefficients is presented on Fig. 8a. In the soil not exposed to root growth soil  $\delta^{13}$ C was positively correlated with 7-15  $\mu$ m and 15-40  $\mu$ m  $\varnothing$  pores, also only prior to the incubation (Fig. 8b).

In the soil with intact structure exposed to plant roots, prior to incubation,  $\delta^{13}$ C signatures were significantly positively associated with presence of the largest pores (>90  $\mu$ m Ø) (Supplemental Fig. 4 reports individual scatter plots, Fig. 8a reports correlation coefficients). After incubation, soil  $\delta^{13}$ C was positively correlated with 15-40  $\mu$ m and 40-90  $\mu$ m Ø pores. In the soil not exposed to plant roots, prior to incubation, soil  $\delta^{13}$ C was negatively correlated with

15-40  $\mu m$  and 40-90  $\mu m$  Ø pores, while there were no significant associations after the incubation (Fig. 8b).

In the soil exposed to plant roots the cumulative amount of  $CO_2$  emitted during incubation was positively correlated with 40-90  $\mu$ m and >90  $\mu$ m Ø pores, while in the soil not exposed to plant roots cumulative  $CO_2$  was negatively correlated with 40-90  $\mu$ m Ø pores (Fig. 9). Likewise, in the soil exposed to plant roots  $\delta^{13}C$  signatures of emitted  $CO_2$  were positively correlated with 40-90  $\mu$ m and >90  $\mu$ m Ø pores. In the soil not exposed to plant roots  $\delta^{13}C$  signatures of emitted  $CO_2$  were positively correlated with 7-15  $\mu$ m Ø pores. Unfortunately, limited number of soil cores used in the incubation experiment precluded exploring the correlations separately by each soil structure type within each root-exposure group.

#### 4. DISCUSSION

The pulse-labeling approach used in this study led to a substantial  $^{13}$ C enrichment of the labeled plants and of the soil exposed to growing plant roots (Fig. 6). While pulse-labeling does not allow calculations of the total amounts of C added by the growing plants to the studied soil, it is a useful tool for assessing relative contributions of different soil management and land use treatments and to study subsequent processing of plant-assimilated C (Kuzyakov and Domanski, 2000; Johnson et al., 2002; Hannula et al., 2012). Here, it enabled comparisons between intact and destroyed soil structures, between soils exposed and non-exposed to root growth, and allowed exploring associations between soil  $\delta^{13}$ C signatures and pores of different sizes.

Destroying the inherent soil structure by sieving expectedly modified pore-size distributions by increasing presence of medium sized pores (15-40  $\mu$ m Ø) and decreasing presence of large pores (>90  $\mu$ m Ø) (Fig. 5). Soil structure differences were further accentuated

by the plants, since active plant growth also changes pore-size distributions (Feeney et al., 2006) both by the physical impact from growing roots and by root exudate additions during plant growth (Zhang et al., 2020). Consistent with previous reports (Valentine et al., 2012), plants grew better in the sieved soil, producing greater above and belowground biomass (Table 1). The differences in plant growth and subsequent modifications in pore-size distributions is what likely led to different patterns in associations between pores and <sup>13</sup>C label in soils with destroyed and intact structures (Fig. 8).

Minimal diameters of plant roots tend to be within a 40  $\mu$ m range and it has been shown that roots can only enter pores of this or greater size (Wiersum, 1957; Cannell, 1977). Roots often preferentially grow into already established pores of old root channels (Rasse and Smucker, 1998; Valentine et al., 2012; Pagenkemper et al., 2013; Zhou et al., 2020). In the soil with intact structure the roots likely took advantage of the greater abundance of large pores (Fig. 5), many of which probably were the former root channels. Thus, larger pores were the places where the root-originated C was likely deposited during the experiment, resulting in the positive correlation between  $\delta^{13}$ C signatures and presence of large pores (>90  $\mu$ m Ø) (Supplement Fig. 4d, Fig 8). Consistent with this result, positive correlations between soil C and presence of large (>120  $\mu$ m Ø) pores within intact macro-aggregates was also reported before (Ananyeva et al., 2013). In the soil with destroyed structure large inherent pores were destroyed by sieving, thus, young rye roots formed new pores, generating the observed positive associations between soil  $\delta^{13}$ C and 40-90  $\mu$ m Ø pores (Fig. 7b and c, Fig. 10). Previous work also has shown that pores of this size range can be associated with new C additions (Quigley et al., 2018).

Besides direct rhizodeposition, plant-assimilated C can be added to the soil via fungi colonizing plant roots (Luginbuehl et al, 2017). Rye is known for developing associations with

arbuscular mycorrhizal fungi; the associations that can get particularly pronounced in the absence of fertilization (Gollner et al., 2011). Fungal mycelia can enter pores comparable with their sizes (>10 µm Ø) and can push aside silt particles to create 20-30 µm Ø pores (Bearden, 2001; Dorioz et al, 1993; Emerson and McGarry, 2003). In soil accessible to fungi the volume of >4-10 µm Ø pores doubled that in non-planted and in fungi non-accessible soil in just 30-50 days (Feeney et al., 2006; Hallett et al., 2009). In the soil with destroyed structure of this study the fungal growth and C transport via fungal hyphae is one of the possible explanations of the increases in new C associated with the 15-40 µm Ø pores (Fig. 8a) as these pores that are too small to host plant roots. Moreover, fungal networks are likely what was responsible for the occurrence of plant-assimilated C in the soil not directly exposed to growing roots (Fig. 6). Fungi actively utilize C-rich plant exudates (Hannula et al., 2012; Kusliene et al., 2014) and can transport C to great distances (Godbold et al, 2006). Positive correlations between soil  $\delta^{13}$ C and 7-15 and 15-40 µm Ø pores in the soil with destroyed structure agree with the fungal transport explanation (Fig. 8b). However, in the soil with intact structure not exposed to plant roots the soil  $\delta^{13}$ C was negatively associated with 15-90 µm Ø pores (Fig. 8b). As mentioned earlier, pores of 15-40 µm Ø size range were much less abundant in the intact soil than in the soil with destroyed structure (Fig. 5b), yet it is not clear why new fungal networks that formed during rye growth in the intact soil seemed to avoid these pores.

390

391

392

393

394

395

396

397

398

399

400

401

402

403

404

405

406

407

408

409

410

411

412

After 21-day incubation substantial amounts of plant-assimilated C were lost and soil  $\delta^{13}$ C signatures dropped, especially sizably in the soil exposed to rye roots (Fig. 6). Incubation differentially affected associations between soil  $\delta^{13}$ C and pores in the soil with disturbed and intact structures. In the sieved soil after incubation all correlations between soil  $\delta^{13}$ C and pores disappeared (Fig. 8). This result is consistent with an earlier report of Quigley et al (2018) and

suggests that in the soil with destroyed structure pores that received new C during plant growth quickly lost it.

The losses of new C from pores of a certain size could be caused by the movement of the added C away from the pores where it was originally deposited, or it can result from decomposition of plant-derived inputs followed by C losses as emitted  $CO_2$ . Positive correlations between 40-90 and >90  $\mu$ m Ø pores with  $CO_2$  emitted during incubation and with  $\delta^{13}C$  signatures of the emitted  $CO_2$  (Fig. 9) suggest that decomposition played a substantial role in decreasing presence of new C in these pores. Pores of this size range have been long known for the greater mineralization of the organics in them (Killham et al., 1993; Strong et al., 2004; Ruamps et al., 2013; Quigley et al., 2018), higher microbial turnover (Killham et al., 1993; Kravchenko et al., 2020), and for being more likely populated by K-strategy microorganisms (Kravchenko et al., 2014; Banfield et al., 2017). However, redistribution of the plant-derived C could be a possible reason of why in the intact soil exposed to plant roots, after incubation, soil  $\delta^{13}C$  became positively associated with 15-90  $\mu$ m Ø pores.

In the soil inaccessible to roots, correlations with pores disappeared after the incubation in the soil of both intact and disturbed structures. Positive correlation between 7-15  $\mu$ m pores and  $\delta^{13}$ C of emitted CO<sub>2</sub> (Fig. 9) is yet further support of the notion that the pores that were associated with greater soil  $\delta^{13}$ C initially (Fig. 8b), were then associated with greater  $\delta^{13}$ C of the lost C. These observations are consistent with earlier findings that plant-assimilated C brought into the soil via arbuscular mycorrhizal fungi networks can be lost to the atmosphere rapidly and in large quantities (Johnson et al., 2002; Huang et al., 2020).

#### 5. CONCLUSIONS

Inherent soil structure differences prior to plant growth, i.e., intact vs. sieved soils of this study, can have a major effect on locations and fate of new photo-assimilated soil C additions. In root-exposed intact-structure soil the additions of new C were associated with >90  $\mu$ m Ø pores, possibly as legacy macro-pores and old root channels. However, in destroyed-structure soils, where large pores and older root channels were not present, new C was positively associated with the 15-90  $\mu$ m Ø pores, potentially indicating preference by plants for these pore sizes when old root channels are missing. In the destroyed-structure soils inaccessible to plant roots,  $\delta^{13}$ C was positively associated with the 7-40  $\mu$ m Ø pores, indicative of its transport via fungal hyphae.

The greater losses of new C tended to occur in those same pores where it was initially preferentially added.  $CO_2$  and  $\delta^{13}C$  of the lost  $CO_2$  associations with pores further support this notion. This may explain why C additions may take years to be observable as new C, even when added in large amounts, may quickly be lost and, therefore, why more biomass does not always equate to C gains.

### Acknowledgements

We are indebted to Jim Muns from Michigan State University's Physics/Astronomy
Research Shop for manufacturing the micro-sampling device and to Dr. Mark Rivers from
Argonne National Laboratory for assistance with scanning the samples. We would like to thank
Ehsan Toosi for advice on pulse-labeling implementation and Emily McKay for her help in
sample preparations.

Support for this research was provided by USDA-NIFA Project "Using stable isotopes and computer tomography to determine mechanisms of soil carbon protection in cover crop based

- agricultural systems", Award No. 2016-67011-24726. Additional support was provided by the
- NSF LTER Program (DEB 1027253) at the Kellogg Biological Station, by Michigan State
- 460 University AgBioResearch, and by USDA NC1187 project. The experiment was performed at
- 461 GeoSoilEnviroCARS (The University of Chicago, Sector 13), Advanced Photon Source (APS),
- 462 Argonne National Laboratory. GeoSoilEnviroCARS is supported by the National Science
- Foundation Earth Sciences (EAR 1634415). This research used resources of the Advanced
- 464 Photon Source, a U.S. Department of Energy (DOE) Office of Science User Facility operated for
- 465 the DOE Office of Science by Argonne National Laboratory under Contract No. DE-AC02-
- 466 06CH11357.

# 467

468

#### REFERENCES

- Abraha, M., Hamilton, S. K., Chen, J., Robertson, G.P., 2018. Ecosystem carbon exchange on
- 470 conversion of Conservation Reserve Program grasslands to annual and perennial cropping
- 471 systems. Agric For Meteorol. 253-254, 151-160.
- 472 https://doi.org/10.1016/j.agrformet.2018.02.016
- 473 Ananyeva, K., Wang, W., Smucker, A.J.M., Rivers, M.L., Kravchenko, A.N., 2013. Can intra-
- aggregate pore structures affect the aggregate's effectiveness in protecting carbon? Soil Biol.
- 475 Biochem. 57, 868-875 https://doi.org/10.1016/j.soilbio.2012.10.019
- Austin, E.E., Wickings, K., McDaniel, M.D., Robertson, G.P., Grandy, S., 2017. Cover crop root contributions to soil carbon in a no-till corn bioenergy cropping system. GCB Bioenergy 9,
- 478 1252-1263. https://doi.org/10.1111/gcbb.12428
- 479 Badri, D.V., Weir, T.L., van der Lelie, D., Vivanco, J.M., 2009. Rhizosphere chemical
- dialogues: plant-microbe interactions. Curr. Opin. Biotechnol. 20, 642-650.
- 481 https://doi.org/10.1016/j.copbio.2009.09.014
- Bailey, V.L., Smith, A.P, Tfaily, M., Fansler, S.J., Bond-Lamberty, B., 2017. Differences in soluble organic carbon chemistry in pore waters sampled from different pore size domains.
- 484 Soil Biol. Biochem. 107, 133-143. https://doi.org/10.1016/j.soilbio.2016.11.025
- Bais, H.P., Weir, T.L., Perry, L.G., Gilroy, S., Vivanco, J.M., 2006. The role of root exudates in rhizosphere interations with plants and other organisms. Annu. Rev.Plant Biol 57, 233-266.
- 487 https://doi.org/10.1146/annurev.arplant.57.032905.105159
- Banfield, C.C., Dippold, M.A., Pausch, J., Hoang, D.T.T., Kuzyakov, Y., 2017. Biopore history
- determines the microbial community composition in subsoil hotspots. Biol. Fertil. Soils 53,
- 490 573-588. https://doi.org/10.1007/s00374-017-1201-5
- Barber, D., Martin J., 1976. Release of organic substances by cereal roots into soil. New Phytol.
- 492 76, 69-80. https://doi.org/10.1111/j.1469-8137.1976.tb01439.x

- Bauer, A., Black A.L., 1994. Quantification of the effect of soil organic matter content on soil
   productivity. Soil Sci. Soc. Am. J. 58, 185-193.
- 495 https://doi.org/10.2136/sssaj1994.03615995005800010027x
- Bearden, B.N. 2001. Influence of arbuscular mycorrhizal fungi on soil structure and soil water
   characteristics of vertisols. Plant Soil 229, 245–258.
   https://doi.org/10.1023/A:1004835328943
- Benard, P., Zarebanadkouki, M., Brax, M., Kaltenbach, R., Jerjen, I., Marone, F., Couradeau, E.,
   Felde, V., Kaestner, A., Carminati, A., 2019. Microhydrological Niches in Soils: How
   Mucilage and EPS Alter the Biophysical Properties of the Rhizosphere and Other Biological
   Hotspots. Vadose Zone J 18. https://doi.org/10.2136/vzj2018.12.0211
- Bengough, A.G., Bransby, M.F., Hans, J. McKenna,S.J., Roberts, T.J., Valentine,T.J., 2006.
   Root responses to soil physical conditions; growth dynamics from field to cell. J. Exp. Bot.
   57, 437-447. https://doi.org/10.1093/jxb/erj003
- Bird, J. A., van Kessel, C., Horwath, W.R., 2003. Stabilization of 13C-carbon and
   immobilization of 15N-nitrogen from rice straw in humic fractions. Soil Sci. Soc. Am. J. 67,
   806-816. https://doi.org/10.2136/sssaj2003.0806
- Bowen, H.D., 1981. Alleviating mechanical impedance. In: G. F. Arkin and H. M. Taylor.
  Editors, Modifying the Root Environment to Reduce Crop Stress. Am. Soc. Agric. Engineers,
  St. Joseph, MI. p. 21-57.
- Brimecombe, M. J., de Leij, F., Lynch, J.M., 2001. The effect of root exudates on rhizosphere microbial populations, in R. Pinton, Z. Varanini and P. Nannipieri, editors, The rhizosphere: biochemistry and organic substances at the soil-plant interface. Marcel Dekker, New York, New York, USA p. 95–140.
- Cannell, R.Q., 1977. Soil aeration and compaction in relation to root growth and soil management. Appl. Biol. 2,1-86.
- Carminati, A., Moradi, A.B., Vetterlein, D., Vontobel, P., Lehmann, E., Weller, U., Vogel, H.J., Oswald, S.E., 2010. Dynamics of soil water content in the rhizosphere. Plant Soil 332, 163-176. https://doi.org/10.1007/s11104-010-0283-8
- Chimento, C., Almagro, M., Amaducci, S., 2016. Carbon sequestration potential in perennial
   bioenergy crops: the importance of organic matter inputs and its physical protection. GCB
   Bioenergy 8, 111-121. https://doi.org/10.1111/gcbb.12232
- Crum, J. R., Collins, H.P., 1995. KBS Soils. W. K. Kellogg Biological Station Long-Term
   Ecological Research Project, Michigan State University, Hickory Corners, MI.
   http://www.lter.kbs.msu.edu/soil/characterization. (accessed 8 Jan. 2018).
- Davidson, E. A., Janssens, I.A., 2006. Temperature sensitivity of soil carbon decomposition and feedbacks to climate change. Nature 440, 165-173. https://doi.org/10.1038/nature04514
- 529 Dexter, A.R. 1987., Compression of soil around roots. Plant Soil 97,401-406. 530 https://doi.org/10.1007/BF02378351
- Dorioz, J.M., Robert, M., Chenu, C., 1993. The role of roots, fungi and bacteria on clay particle organization. An experimental approach. Geoderma 56, 179–194. https://doi.org/10.1016/0016-7061(93)90109-X
- Dungait, J.A.J., Hopkins, D.W., Gregory, A.S., Whitmore, A.P., 2012. Soil organic matter turnover is governed by accessibility not recalcitrance. Global Change Biol. 18, 1781-1796. https://doi.org/10.1111/j.1365-2486.2012.02665.x
- Ekschmitt, K., Kandeler, E., Poll, C., Brune, A., Buscot, F., Friedrich, M., Gleixner, G., Hartmann, A., Kästner, M., Marhan, S., Miltner, A., Scheu, S., Wolters, V., 2008. Soil-

- carbon preservation through habitat constraints and biological limitations on decomposer activity. J. Plant Nutr. Soil Sci. 171, 27-35. https://doi.org/10.1002/jpln.200700051
- Ekschmitt, K., Liu, M., Vetter, S., Fox, O., Wolters, V., 2005. Strategies used by soil biota to overcome soil organic matter stability why is dead organic matter left over in soil?

  Geoderma 128, 167-176. https://doi.org/10.1016/j.geoderma.2004.12.024
- Emerson, W.W., McGarry, D., 2003. Organic carbon and soil porosity. Aust. J. Soil Res. 41,
   107–118. https://doi.org/10.1071/SR01064
- Falkowski, P., Scholes, R.J., Boyle, E., Canadell, J., Canfield, D., Elser, J., Gruber, N., Hibbard,
  K., Högberg, P., Linder., S., Mackenzie, F.T., Moore III, B., Pedersen, T., Rosenthal, Y.,
  Seitzinger, S., Smetacek, V., Steffen, W., 2000. The global carbon cycle: a test of our
  knowledge of Earth as a system. Science. 290, 291-296.
  https://doi.org/10.1073/pnas.0811302106
- Feeney, D.S., Crawford, J.W., Daniell, T., Hallett, P.D., Nunan, N., Ritz, K., Rivers, M., Young,
   I.M., 2006. Three-dimensional microorganization of the soil-root-microbe system. Microb.
   Ecol. 52, 151-158. https://doi.org/10.1007/s00248-006-9062-8
- Gale, W.J., Cambardell, C.A., Bailey, T.B., 2000. Surface residue- and root-derived organic
   matter under simulated no-till. Soil Sci. Soc. Am. J. 64, 196-201.
   https://doi.org/10.2136/sssaj2000.641196x
- Garten, C.T., Wullschleger, S.D., 1999. Soil carbon inventories under a bioenergy crop
   (switchgrass): measurement limitations. J Environ. Qual 28, 1359-1365.
   https://doi.org/10.1016/j.biombioe.2010.08.013
- Godbold, D.L., Hoosbeek, M.R., Lukac, M., Cotrufo, M.F., Janssens, I.A., Ceulemas, R., Polle,
   A., Velthorst, E. J., Scarascia-Mugnozza, G., De Angelis, P., Miglieta, F., Peresotti, A., 2006.
   Mycorrhizal hyphal turnover as a dominant process for carbon input into soil organic matter.
   Plant Soil 281, 15-24. https://doi.org/10.1007/s11104-005-3701-6
- Gollner, M.J., Wagentristl, H., Liebhard, P., Friedel, J.K., 2011. Yield and arbuscular mycorrhiza
   of winter rye in a 40-year fertilisation trial. Agron Sustain Dev 31, 373-378.
   https://doi.org/10.1051/agro/2010032
- Graecen, E.L., Farrell, D.A., Cockroft, B., 1968. Soil resistance to metal probes and plant roots.
   9th International Congress of Soil Science, Angus and Roberton, Adelaide. 769-779.
- Grandy, A.S., Neff, J.C., 2008. Molecular C dynamics downstream: the biochemical
   decomposition sequence and its impact on soil organic matter structure and function. Sci
   Total Environ 404, 297-307. https://doi.org/10.1016/j.scitotenv.2007.11.013
- Grandy, A.S., Robertson, G.P., 2007. Land-use intensity effects on soil organic carbon
   accumulation rates and mechanisms. Ecosystems 10, 58-73. https://doi.org/10.1007/s10021-006-9010-y
- Hallett, P.D., Feeney, D.S., Bengough, A.G., Rillig, M.C., Scrimgeour, C.M., Young, I.M., 2009.
   Disentangling the impact of AM fungi versus roots on soil structure and water transport.
   Plant Soil 314, 183-196. https://doi.org/10.1007/s11104-008-9717-y
- Hannula, S.E., Boschker, H.T.S., de Boer, W., van Veen, J.A., 2012. 13C pulse-labeling assessment of the community structure of active fungi in the rhizosphere of a genetically starch-modified potato (Solanum tuberosum) cultivar and its parental isoline. New Phytol. 194, 784-799. https://doi.org/10.1111/j.1469-8137.2012.04089.x
- Huang, J.S., Liu, W.X., Deng, M.F., Wang, X., Wang, Z.H., Yang, L., Liu, L.L., 2020.
   Allocation and turnover of rhizodeposited carbon in different soil microbial groups. Soil Biol
   Biochem 150. https://doi.org/10.1016/j.soilbio.2020.107973

- Jackson, R.B., Lajtha, K., Crow, S.E., Hugelius, G., Kramer, M.G., Piñeiro, G., 2017. The ecology of soil carbon: pools, vulnerabilities, and biotic and abiotic controls. Annu Rev Ecol Evol Syst. 48, 419-445. https://doi.org/10.1146/annurev-ecolsys-112414-054234
- Johnson, D., Leake, J.R., Ostle, N., Ineson, P., Read, D.J., 2002. In situ (CO2)-C-13 pulse-labelling of upland grassland demonstrates a rapid pathway of carbon flux from arbuscular mycorrhizal mycelia to the soil. New Phytol. 153, 327-334. https://doi.org/10.1046/j.0028-646X.2001.00316.x
- Kallenbach, C.M., Frey, S,D., Grandy, A.S., 2016. Direct evidence for microbial-derived soil
   organic matter formation and its ecophysiological controls. Nat. Commun. 7, 13630.
   https://doi.org/10.1038/ncomms13630
- Kallenbach, C.M., Grandy, A.S., Frey, S.D., Diefendorf, A.F., 2015. Microbial physiology and necromass regulate agricultural soil carbon accumulation. Soil Biol. Biochem 9, 279-290. https://doi.org/10.1016/j.soilbio.2015.09.005
- Keiluweit, M., Wanzek, T., Kleber, M., Nico, P., Fendorf, S. 2017. Anaerobic microsites have an unaccounted role in soil carbon stabilization. Nat. Commun. 8, 171. https://doi.org/10.1038/S41467-017-01406-6
- Kell, D.B., 2012. Large-scale sequestration of atmospheric carbon via plant roots in natural and
   agricultural ecosystems: why and how. Philos T R Soc B. 367, 1589-1597.
   https://doi.org/10.1098/rstb.2011.0244
- Killham, K., Amato, M., Ladd, J.N., 1993. Effect of Substrate Location in Soil and Soil Pore Water Regime on Carbon Turnover. Soil Biol Biochem 25, 57-62.
   https://doi.org/10.1016/0038-0717(93)90241-3
- Koebernick, N., Daly, K.R., Keyes, S.D., Bengough, A.G., Brown, L.K., Cooper, L.J., George, T.S., Hallett, P.D., Naveed, M., Raffan, A., Roose, T., 2019. Imaging microstructure of the barley rhizosphere: particle packing and root hair influences. New Phytol. 221, 1878-1889. https://doi.org/10.1111/nph.15516
- Koebernick, N., Daly, K.R., Keyes, S.D., George, T.S., Brown, L.K., Raffan, A., Cooper, L.J.,
   Naveed, M., Bengough, A.G., Sinclair, I., Hallett, P.D., Roose, T., 2017. High-resolution
   synchrotron imaging shows that root hairs influence rhizosphere soil structure formation.
   New Phytol. 216, 124-135. https://doi.org/10.1111/nph.14705
- Kong, A.Y.Y., Six, J., 2010. Tracing root vs. residue carbon into soils from conventional and alternative cropping systems. Soil Sci. Soc. Am. J. 74, 1201-1210. https://doi.org/10.2136/sssaj2009.0346
- Kravchenko, A.N., Guber, A. K., 2017. Soil pores and their contributions to soil carbon processes. Geoderma 287, 31-39. https://doi.org/10.1016/j.geoderma.2016.06.027
- Kravchenko, A.N., Guber, A.K., Gunina, A., Dippold, M., Kuzyakov, Y., 2021. Pore- scale view
   of microbial turnover: combining 14C imaging, μCT, and zymography after adding soluble
   carbon to soil pores of specific sizes. Eur. J. Soil Sci. 72, 593-607
   https://doi.org/10.1111/ejss.13001.
- Kravchenko, A.N., Negassa, W.C., Guber, A.K., Hildebrandt, B., Marsh, T.L., Rivers, M.L.,
   2014. Intra-aggregate pore structure influences phylogenetic composition of bacterial
   community in macroaggregates. Soil Sci. Soc. Am. J. 78, 1924-1939.
   https://doi.org/10.2136/sssaj2014.07.0308
- Kravchenko, A.N., Negassa, W.C., Guber, A.K., Rivers, M.L., 2015. Protection of soil carbon within macro-aggregates depends on intra-aggregate pore characteristics. Sci. Rep. 5, 16261. https://doi.org/10.1038/srep16261

- Kušlienė, G., Rasmussen, J., Kuzyakov, Y., Eriksen, J., 2014. Medium-term response of
- microbial community to rhizodeposits of White clover and ryegrass and tracing of active
- processes induced by C-13 and N-15 labelled exudates. Soil Biol Biochem 76, 22-33.
- https://doi.org/10.1016/j.soilbio.2014.05.003
- 635 Kuzyakov, Y., 2002. Review: Factors affecting rhizosphere priming effects. J. Plant. Nutr. Soil Sci. 165, 382-396. https://doi.org/10.1002/1522-2624(200208)165:4<382::AID-JPLN382>3.0.CO;2-%23
- 638 Kuzyakov, Y., Domanski, G., 2000. Carbon input by plants into the soil. Review. J. Plant. Nutr. 639 Soil Sci. 163, 421-431. https://doi.org/10.1002/1522-2624(200008)163:4<421::AID-JPLN421>3.0.CO;2-R
- Kuzyakov, Y., Leinweber, P., Sapronov, D., Eckhardt, K.U., 2003. Qualitative assessment of
   rhizodeposits in non-sterile soil by analytical pyrolysis. J. Plant Nutr. 166, 719-723.
   https://doi.org/10.1002/jpln.200320363
- Lal, R., 1999. Soil management and restoration for carbon sequestration to mitigate the accelerated greenhouse effect. Prog. Env. Sci. 1, 307-326. https://doi.org/10.1055/s-2008-1072270
- 647 Lal, R., 2006. Enhancing crop yields in the developing countries through restoration of the soil organic carbon pool through restoration of the soil organic carbon pool in agricultural lands.

  649 Land Degrad. Develop. 17, 197-209. https://doi.org/10.1002/ldr.696
- Lal, R., 2011. Sequestering carbon in soils of agro-ecosystems. Food Policy. 36, S33-S39. https://doi.org/10.1016/j.foodpol.2010.12.001
- Lindquist, W.B., Venkatarangan, A., Dunsmuir, J., Wong, T., 2000. Pore and throat size distributions measured from synchrotron X-ray tomographic images of Fontainebleau sandstornes. J. Geophys. Res. 105, 21,509-21,527. https://doi.org/10.1029/2000JB900208
- Lucas, M., Schluter, S., Vogel, H.J., Vetterlein, D., 2019. Roots compact the surrounding soil depending on the structures they encounter. Sci. Rep. 9, 16236 https://doi.org/10.1038/s41598-019-52665-w
- Luehmann, M.D., Peter, B.G., Connallon, C.B., Schaetzl, R.J., Smidt, S.J., Liu, W., Kincare,
   K.A., Walkowiak, T.A., Thorlund, E., Holler, M.S., 2016. Loamy, two-storied soils on the
   outwash plains of southwestern lower Michigan: Pedoturbation of loess and the underlying
   sand. Ann Am Assoc Geogr. 106, 551-572. https://doi.org/10.1080/00045608.2015.1115388
- Luginbuehl, L.H., Menard, G.N., Kurup, S., Van Erp, H., Radhakrishnan, G.V., Breakspear, A.,
   Oldroyd, G.E.D., Eastmond, P.J., 2017. Fatty acids in arbuscular mycorrhizal fungi are
   synthesized by the host plant. Science. 356, 1175-1178.
   https://doi.org/10.1126/science.aan0081
- Mazzilli, S.R., Kemanian, A.R., Ernst, O.R., Jackson, R.B., Piñero, G., 2015. Greater
   humification of belowground than aboveground biomass carbon into particulate soil organic
   matter in no-till corn and soybean crops. Soil Bio. Biochem. 85, 22-30.
   https://doi.org/10.1016/j.soilbio.2015.02.014
- Meharg, A.A., Killham, K., 1991. A novel method of quantifying root exudation in the presence of soil microflora. Plant Soil 113, 111-116. https://doi.org/10.1007/BF00010488
- 672 Melsted, S.W., 1954. New concepts of management of corn belt soils. Adv. Agron. 6, 121-142. 673 https://doi.org/10.1016/S0065-2113(08)60383-1
- Milliken, G A., Johnson, D.E., 2009. Analysis of Messy Data Volume I: Designed Experiments,
   2nd ed. CRC Press, Boca Raton, FL.

- Necpálová, M., Anex Jr., R.P., Kravchenko, A.N., Abendroth, L.J., Del Grosso, S.J., Dick, W.A.,
- Hlmers, M.J., Herzmann, D., Lauer, J.G., Nafziger, E.D., Sawyer, J.E., Scharf, P.C., Strocl,
- J.S., Villamil, M.B., 2014. What does it take to detect a change in soil carbon stock? A
- regional comparison of minimum detectable difference and experiment duration in the north central United States. J Soil Water Conserv. 69, 517-531.
- https://doi.org/10.2489/jswc.69.6.517
- Oechel, W.C., Vourlitis, G.L., 1994. The effects of climate change on land-atmosphere feedbacks in arctic tundra regions. Trends Ecol Evol. 9, 324-329. https://doi.org/10.1016/0169-5347(94)90152-X
- 685 Oh, W., Lindquist, W.B., 1999. Image thresholding by indicator kriging. IEEE Trans. Pattern Anal. Mach. Intell. 21, 590-602. https://doi.org/10.1109/34.777370
- Pagenkemper, S.K., Peth, S., Puschmann, D.U., Horn, R., 2013. Effects of Root-Induced Biopores on Pore Space Architecture Investigated with Industrial X-Ray Computed Tomography, In: Anderson, S.H., Hopmans, J.W. (Eds.), Soil-Water-Root Processes: Advances in Tomography and Imaging, pp. 69-96.
- Park, E.J., Sul, W.J., Smucker, A.J.M., 2007. Glucose additions to aggregates subjected to drying and wetting cycles promote carbon sequestration and aggregate stability. Soil Biol. Biochem. 39, 2758-2768. https://doi.org/10.1016/j.soilbio.2007.06.007
- Pausch, J., Zhu, B., Kuzyakov, Y., Cheng, W., 2013. Plant inter-species effects on rhizosphere priming of soil organic matter decomposition. Soil Bio. Biochem. 57, 91-99. https://doi.org/10.1016/j.soilbio.2012.08.029
- 697 Paustian, K., Lehmann, J., Ogle, S., Reay, D., Robertson, G.P., Smith, P., 2016. Climate-smart soils. Nature 532, 49-57. https://doi.org/10.1038/nature17174
- Quigley, M.Y., Negassa, W.C., Guber, A.K., Rivers, M.L., Kravchenko, A.N., 2018. Influence
   of pore characteristics on the fate and distribution of newly added carbon. Front. Environ.
   Sci. 6, 51. https://doi.org/10.3389/fenvs.2018.00051
- Rabot, E., Wiesmeier, M., Schlüter, S., Vogel, H.-J., 2018. Soil structure as an indicator of soil functions: a review. Geoderma 314, 122-137.
   https://doi.org/10.1016/j.geoderma.2017.11.009
- Rasse, D.P., Rumpel, C., and Dignac, M.-F., 2005. Is soil carbon mostly root carbon?
   Mechanisms for a specific stablisation. Plant Soil 269, 341-356.
   https://doi.org/10.1007/s11104-004-0907-y
- Rasse, D.P., Smucker, A.J.M., 1998. Root recolonization of previous root channels in corn and alfalfa rotations. Plant Soil 204, 203-212. https://doi.org/10.1023/A:1004343122448
- Rivers, M.L., 2012. tomoRecon: High-speed tomography reconstruction on workstations using multi-threading. Proc. SPIE 8505:OU. https://doi.org/10.1117/12.930022
- Rorick, J.D., Kladivko, E.J., 2017. Cereal rye cover crop effects on soil carbon and physical
   properties in southeastern Indiana. J Soil Water Conserv. 72, 260-265.
   https://doi.org/10.2489/jswc.72.3.260
- Ruamps, L.S., Nunan, N., Chenu, C., 2011. Microbial biogeography at the soil pore scale. Soil Biol. Biochem. 43, 280-286. https://doi.org/10.1016/j.soilbio.2010.10.010
- Raun, L., Robertson, G.P., 2013. Initial nitrous oxide, carbon dioxide, and methane costs of converting Conservation Reserve Program grassland to row crops under no-till vs.
- 719 conventional tillage. Global Change Biol. 19, 2478-2489. https://doi.org/10.1111/gcb.12216
- 720 SAS Inc., 2009. SAS user's guide. Verssion 9.2. SAS Inst., Cary, NC

- Senthilkumar, S., Basso, B., Kravchenko, A.N., Robertson, G.P., 2009. Contemporary evidence
   of soil carbon loss in the U.S. corn belt. Soil Sci. Soc. Am. J. 73, 2078-2086.
   https://doi.org/10.2136/sssaj2009.0044
- Sprunger C.D., Robertson, G.P., 2018. Early accumulation of active fraction soil carbon in newly
   established cellulosic biofuel systems. Geoderma 318, 42-51.
   https://doi.org/10.1016/j.geoderma.2017.11.040
- Strong, D.T., De Wever, H., Merckx, R., Recous, S., 2004. Spatial location of carbon decomposition in the soil pore system. Eur. J. Soil Sci. 55, 739-750.
  https://doi.org/10.1111/j.1365-2389.2004.00639.x
- 730 Swift, R.S., 2001. Sequestration of carbon by soil. Soil Sci. 166, 858-871. 731 https://doi.org/10.1097/00010694-200111000-00010
- Syswerda, S.P., Corbin, A.T., Mokma, D.L., Kravchenko, A.N., Robertson, G.P., 2011.
   Agricultural management and soil carbon storage in surface vs. deep layers. Soil Sci. Soc.
   Am. J. 75, 92-101. https://doi.org/10.2136/sssaj2009.0414
- Toosi, E.R., Kravchenko, A.N., Guber, A.K., Rivers, M.L., 2017. Pore characteristics regulate
   priming and fate of carbon from plant residue. Soil Biol. Biochem. 113, 219-230.
   https://doi.org/10.1016/j.soilbio.2017.06.014
- Valentine, T.A., Hallett, P.D., Binnie, K., Young, M.W., Squire, G.R., Hawes, C., Bengough,
   A.G., 2012. Soil strength and macropore volume limit root elongation rates in many UK
   agricultural soils. Ann. Bot. 110, 259-270. https://doi.org/10.1093/aob/mcs118
- Wang, W., Kravchenko, A.N., Johnson, T., Srinivasan, S., Ananyeva, K.A. Smucker, A.J.M.,
   Rose, J.B., Rivers, M.L., 2013. Intra-aggregate pore structures and Escherichia coli
   distribution by water flow within and movement out of soil macroaggregates. Vadose Zone J.
   4. https://doi.org/10.2136/vzj2013.01.0012
- Wang, W., Kravchenko, A.N., Smucker, A.J.M., Liang, W., Rivers, M.L., 2012. Intra-aggregate
   pore characteristics: X-ray computed microtomography analysis. Soil Sci. Soc. Am. J. 76,
   1159-1171. https://doi.org/10.2136/sssaj2011.0281
- Wang, W., Kravchenko, A.N., Smucker, A.J.M., Rivers, M.L., 2011. Comparison of image
   segmentation methods in simulated 2D and 3D microtomographic images of soil aggregates.
   Geoderma. 162, 231-241. https://doi.org/10.1016/j.geoderma.2011.01.006
- Wieder, W.R., Grandy, A.S., Kallenback, C.M., Bonan, G.B., 2014. Integrating microbial physiology and physiochemical principles in soils with MIcorbial-MIneral carbon stabilization (MIMICS) model. Biogeosci. Discuss. 11, 1147-1185.
   https://doi.org/10.5194/bgd-11-1147-2014
   Wiersum, L.K., 1957. The relationship of the size and structural rigidity of pores to their
- Wiersum, L.K., 1957. The relationship of the size and structural rigidity of pores to their penetration by roots. Plant Soil 9, 75-85. https://doi.org/10.1007/BF01343483
- Williams, M.A., Myrold, D.D., Bottomley, P.J., 2006. Distribution and fate of 13C-labeled root and straw residues from ryegrass and crimson clover in soil under western Oregon field conditions. Biol. Fertil. Soils 42, 523-531. https://doi.org/10.1007/s00374-005-0046-5
- Young, I.M., Crawford, J.W., Rappoldt, C., 2001. New methods and models for characterizing
   structural heterogeneity of soil. Soil Tillage Res. 61, 33-45. https://doi.org/10.1016/S0167-1987(01)00188-X
- Zhang, W., Gao, W., Whalley, W.R., Ren, T., 2021. Physical properties of a sandy soil as
   affected by incubation with a synthetic root exudate: Strength, thermal and hydraulic
   conductivity, and evaporation. Eur. J. Soil Sci. 72, 782-792.
- 766 https://doi.org/10.1111/ejss.13007

Zhou, H., Whalley, W.R., Hawkesford, M.J., Ashton, R.W., Atkinson, B., Atkinson, J.A.,
 Sturrock, C.J., Bennett, M.J., Mooney, S.J., 2021. The interaction between wheat roots and soil pores in structured field soil. J. Exp. Bot. 72, 747-756.
 https://doi.org/10.1093/jxb/eraa475

772

**Tables** 

Table 1. Basic soil properties and plant biomass in the soils with destroyed and intact structures.

Shown are means and standard errors.

Sail and plant characteristics	Structure		
Soil and plant characteristics	Intact	Destroyed	Standard error
Bulk Density, g/cm <sup>3</sup>	1.43	1.46	0.03
$\delta^{13}$ C of control soil	-22.8	-22.9	0.4
Total C, %	0.73	0.72	0.02
Total N, %	0.08	0.08	0.003
Aboveground biomass, g/m <sup>2</sup>	75	134	22
Belowground biomass, g/m <sup>2</sup>	126	289	130
δ <sup>13</sup> C of labeled roots	571	522	66

**Figure 1**. Schematic of the experimental design. Soil was collected and then either placed into containers after sieving or undisturbed as much as possible (intact). Root exclusion areas (brown) were created and rye plants planted (green) into both soils. After three months of plant labeling with  $\delta^{13}$ C, samples were collected and scanned from both soils. Half of the samples were sampled for  $\delta^{13}$ C analysis, while the other half were incubated, rescanned, and then sampled for  $\delta^{13}$ C analysis. Details of the sampling process for  $\delta^{13}$ C can be found in Figure 2.

Figure 1: Color Please.

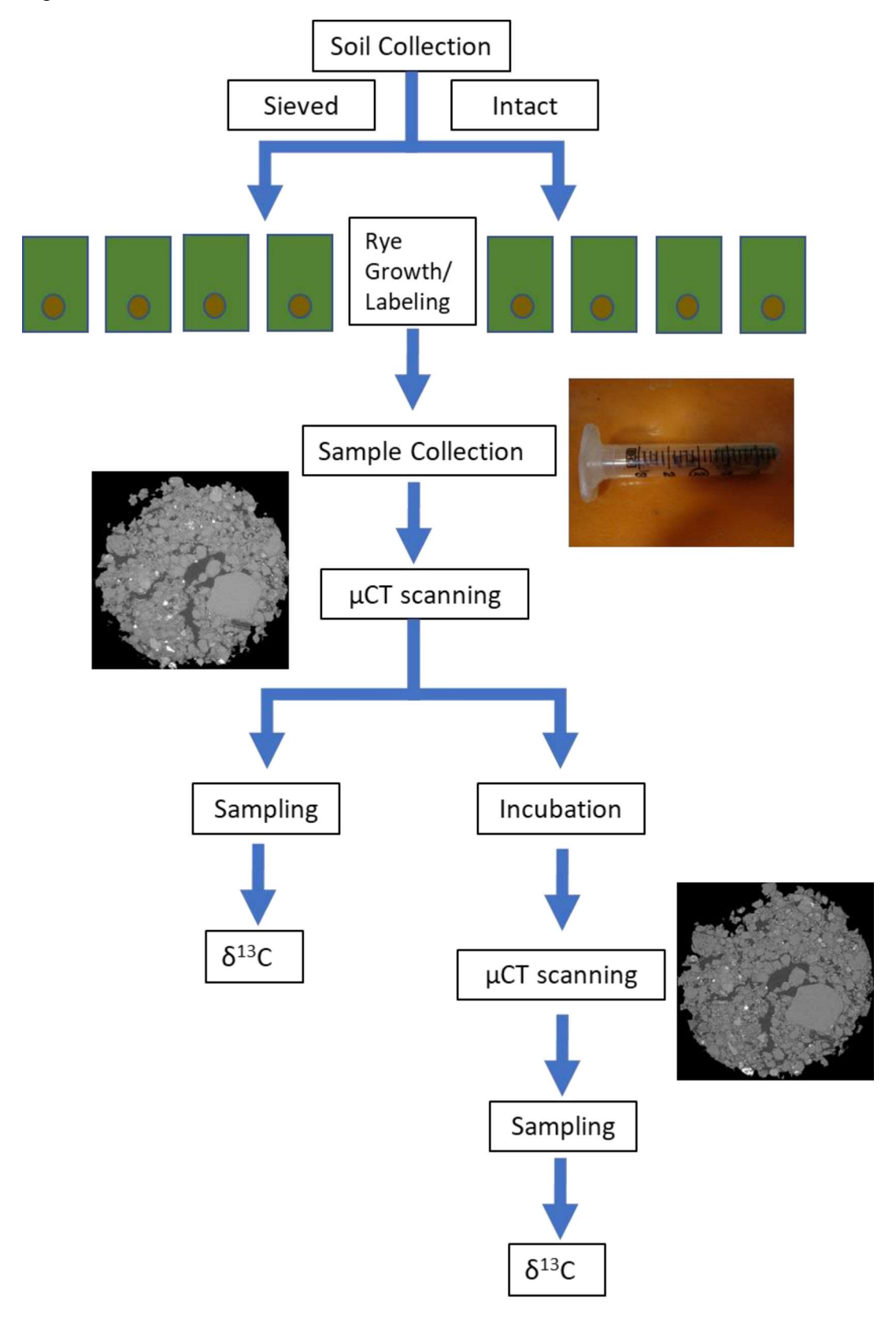
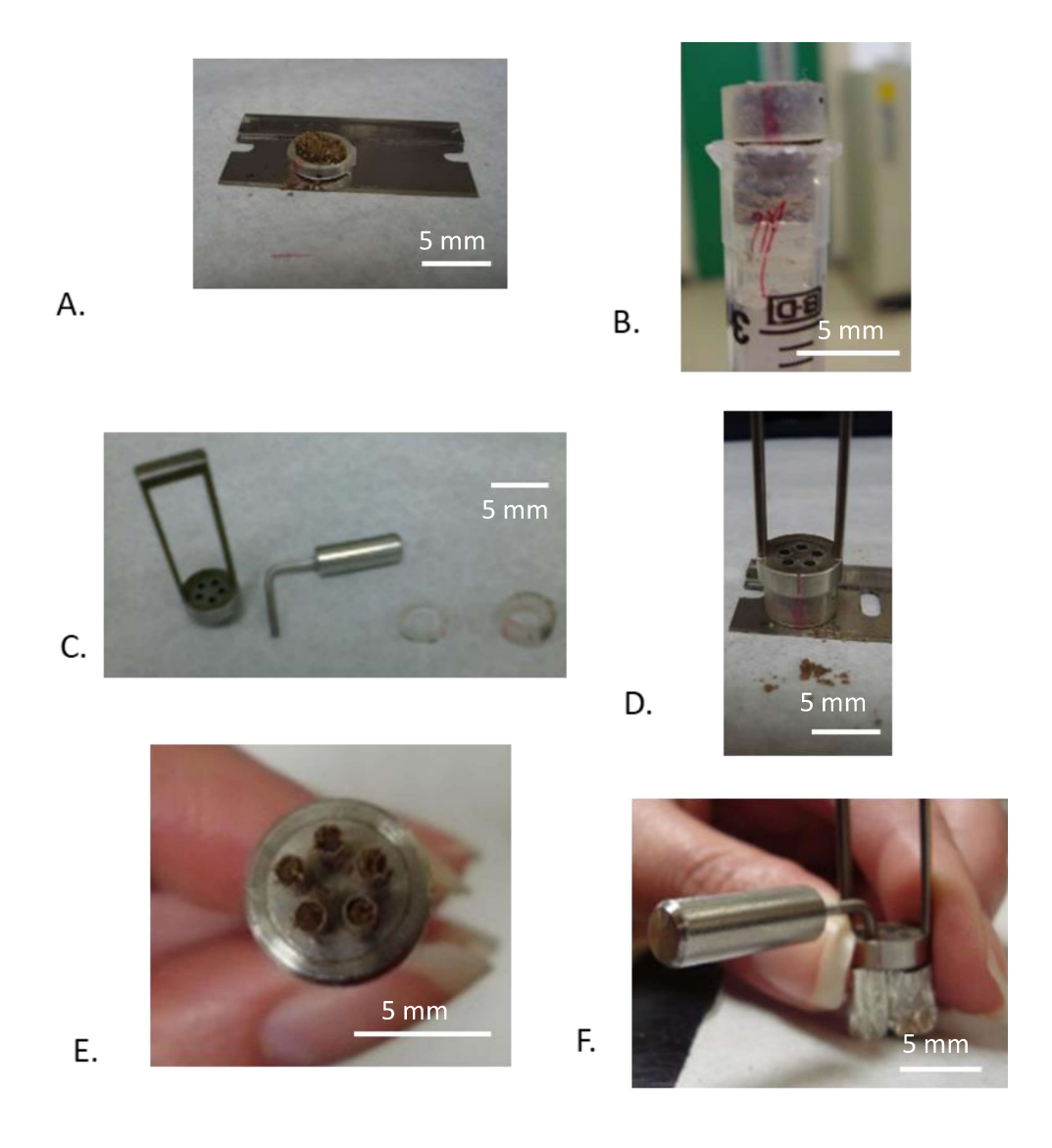


Figure 2. A schematic representation of the steps of soil sampling via the micro-sample device. First, the top 2 mm of the sample is removed and discarded (A). Then the remaining sample is pushed into a 5 mm sample ring and cut (B). The soil sampling device (C) is then aligned with the red mark (D) and five samples collected simultaneously (E). The samples are placed into tins for total C and  $\delta^{13}$ C analysis (F).

Figure 2: Color Please.



**Figure 3**. Selected representative CT images. A whole sample with the subsections taken from the soil sampling device (Fig. 2) overlayed in red (A). Subsample sections taken from the intact without roots (B), intact with roots (C), sieved without roots (D), and sieved with roots (E) samples.

Figure 3: Color please.

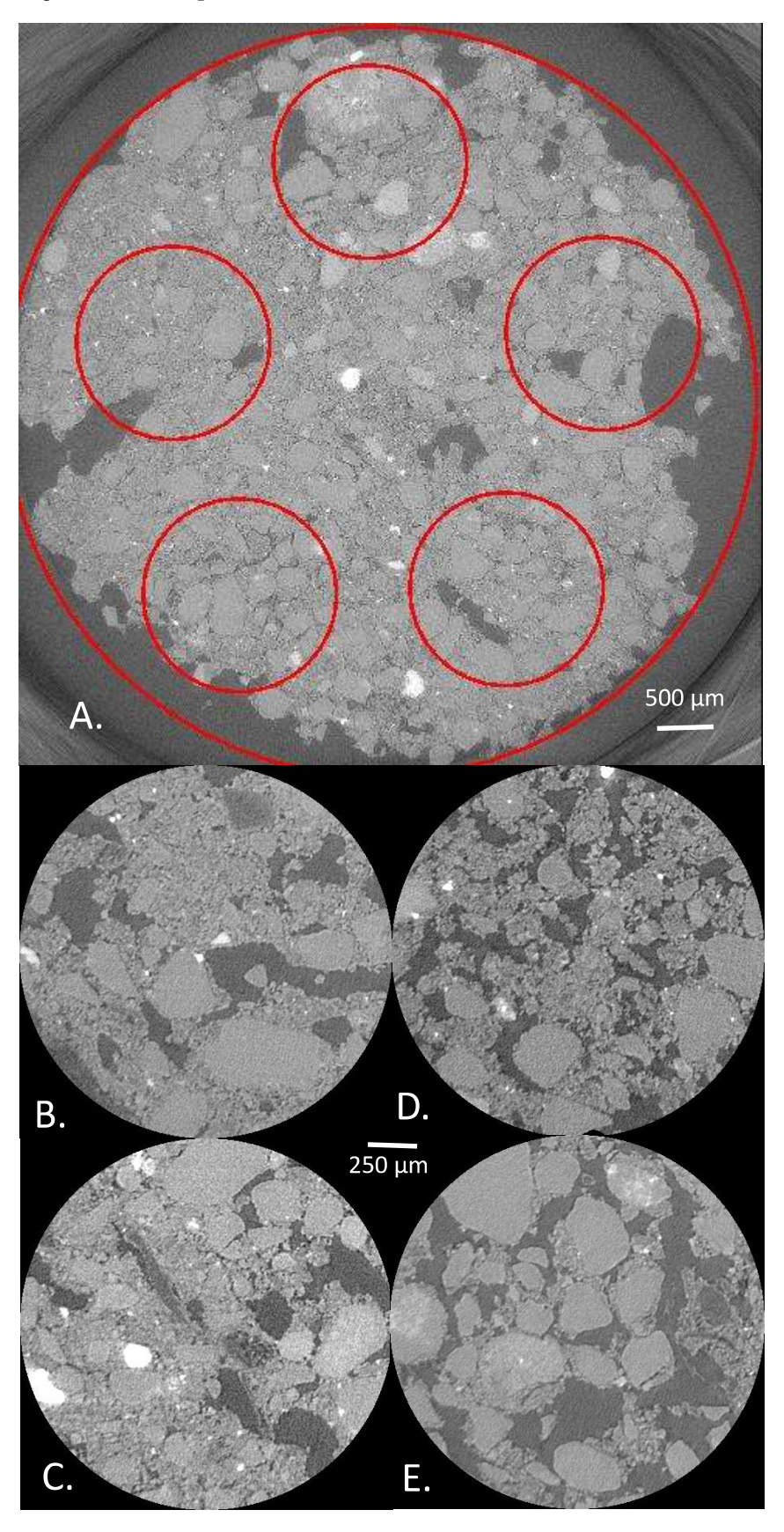


Figure 4. Image based porosity (pores> 7  $\mu$ m Ø) in undisturbed cores subsections from soil with destroyed and intact structure collected in the areas exposed and non-exposed to plant roots and scanned before (Pre) and after (Post) a 21-day incubation. Error bars represent standard errors. Stars mark differences between root exposed and non-exposed soils within each structure and time significant at p<0.05. Upper case letters mark differences between the cores before and after incubation within each structure and root exposure group significant at p<0.05.

Figure 4: Color please

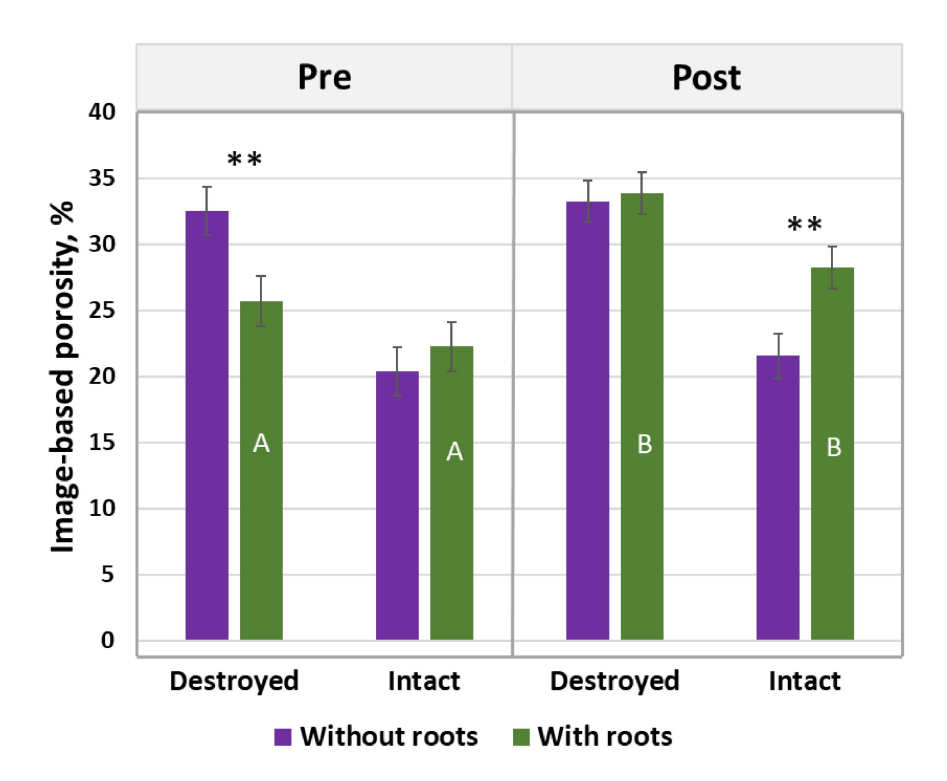
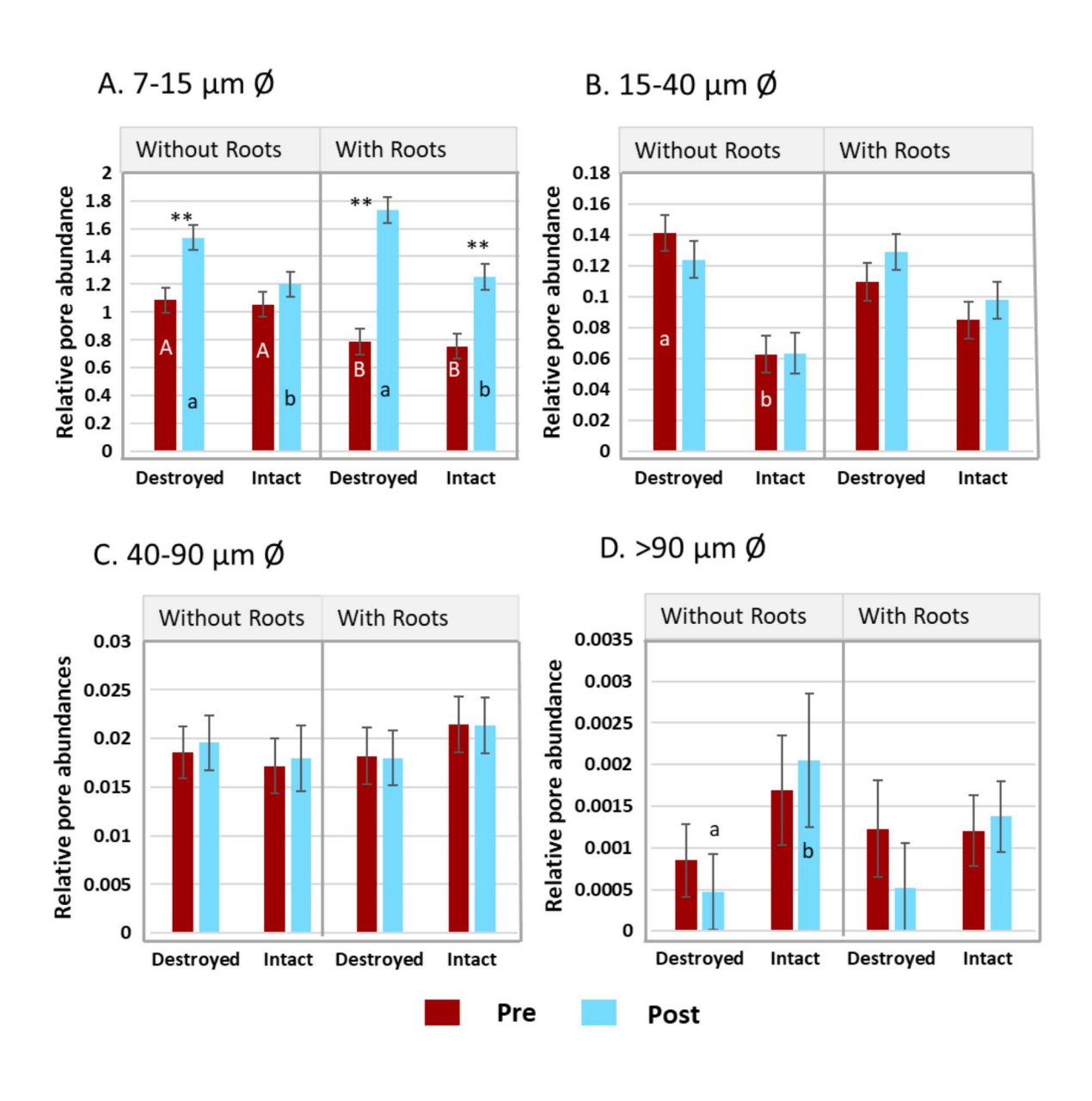


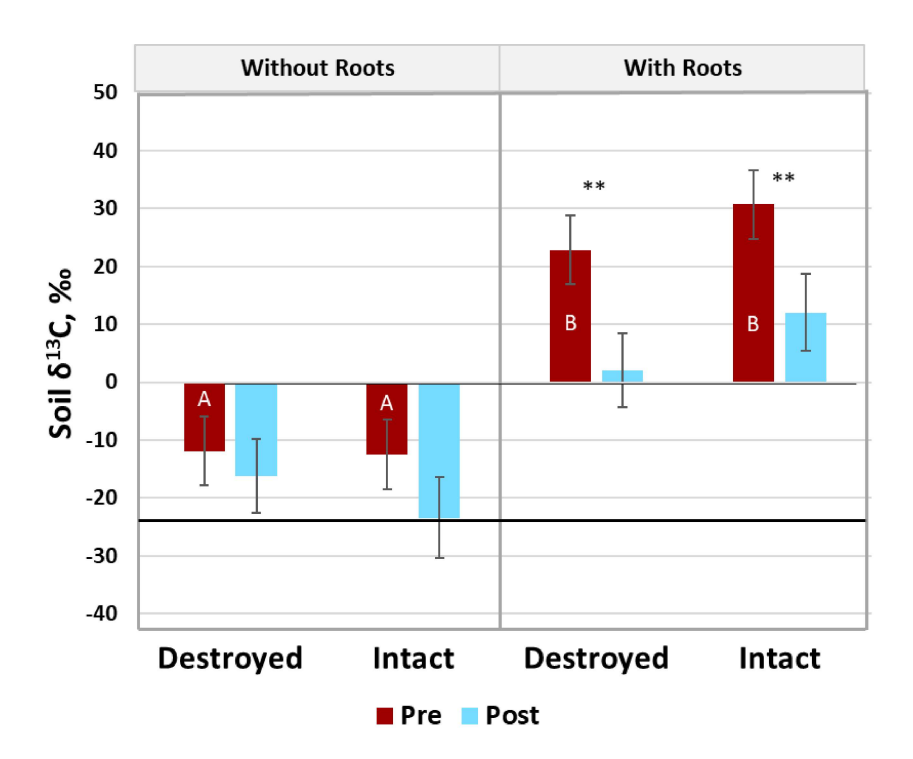
Figure 5. Relative abundances of 7–15 (A), 15–40 (B), 40–90 (C), and >90 μm (D) Ø pores in the undisturbed cores subsections from soils with destroyed and intact structure scanned before (Pre) and after (Post) a 21-day incubation. Relative pore abundance refers to the percent of medial axes per total soil volume as determined from 3DMA-Rock software. Vertical bars represent standard errors. Stars mark differences between the Pre and Post incubation soils significant at p<0.05. Upper case letters mark the differences between the soils exposed and non-exposed to roots significant at p<0.05. Lower case letters mark differences between intact and destroyed structure soils within each incubation and root exposure category at p<0.05.

Figure 5: Color Please



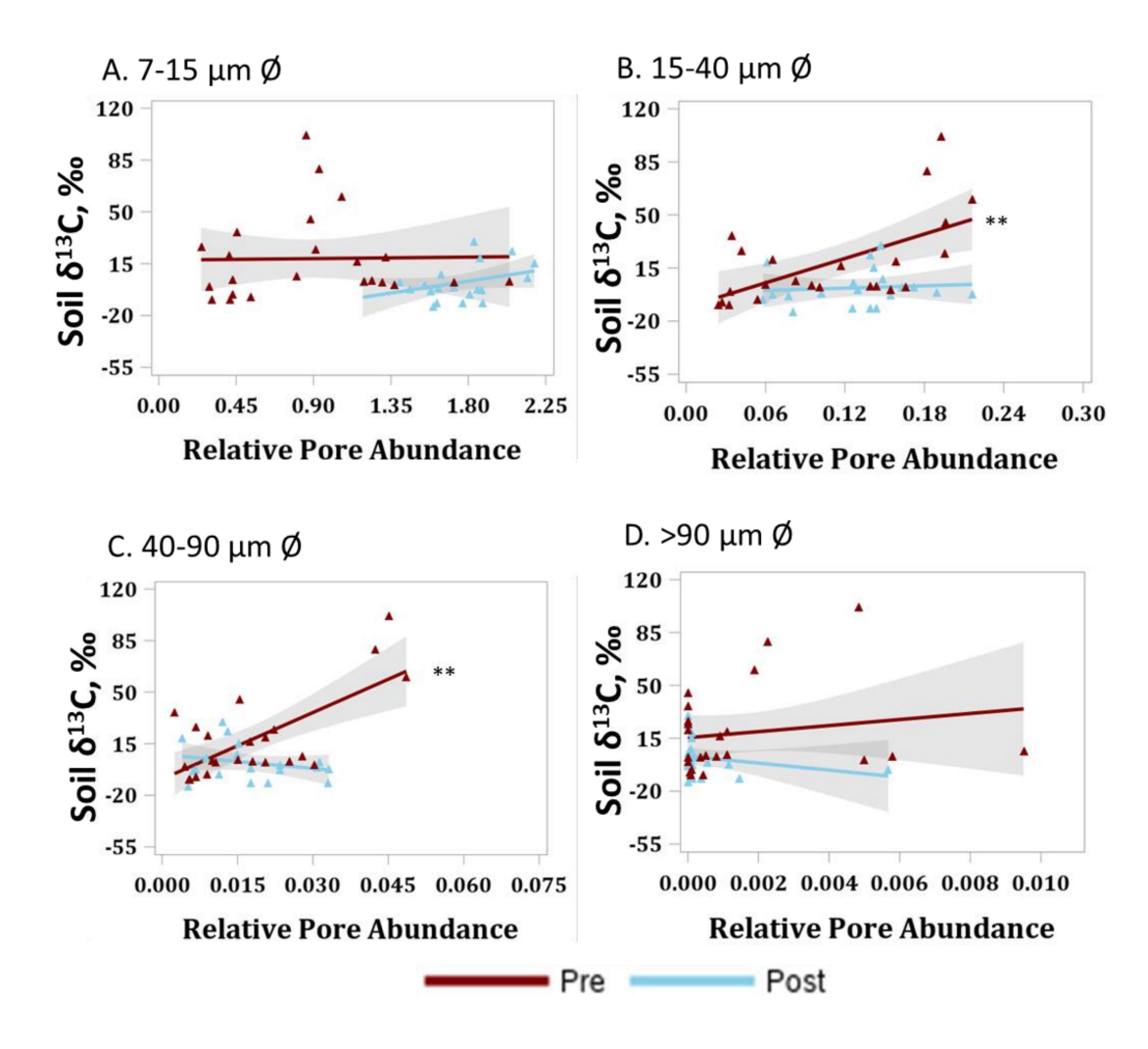
**Figure 6**. The  $\delta^{13}$ C signatures of soils with destroyed and intact structure exposed and non-exposed to roots immediately after plant termination (Pre) and after a 21-day incubation (Post). Shown are means and standard errors (error bars). Horizontal black line marks the  $\delta^{13}$ C signature of the unlabeled soil. Stars mark the cases where Pre and Post values were significantly different from each other at p<0.05. Uppercase letters mark differences between soils exposed and not exposed to roots significant at p<0.05.

Figure 6: Color please.



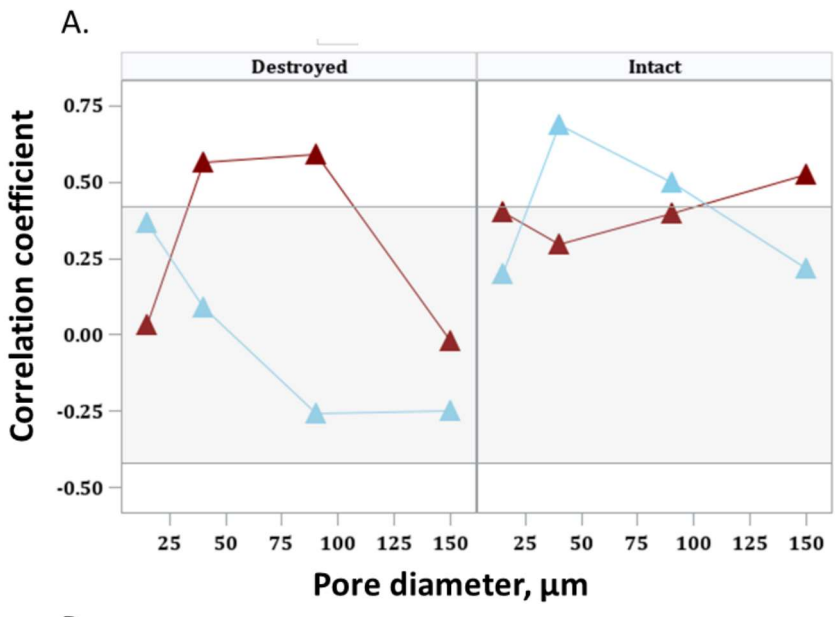
**Figure 7**. Associations between soil  $\delta^{13}$ C and relative abundances of 7–15μm Ø (**A**), 15-40 μm Ø (**B**), 40-90 μm Ø (**C**), and >90 μm Ø (**D**) pores for soils with destroyed structure exposed to growing plant roots before (red) and after (blue) a 21-day incubation. Relative pore abundances refer to the percent of medial axes per total soil volume as determined from 3DMA-Rock software. Stars next to the line ends mark regression slopes significantly different from zero at p<0.05. Gray areas represent 95% confidence intervals for the means.

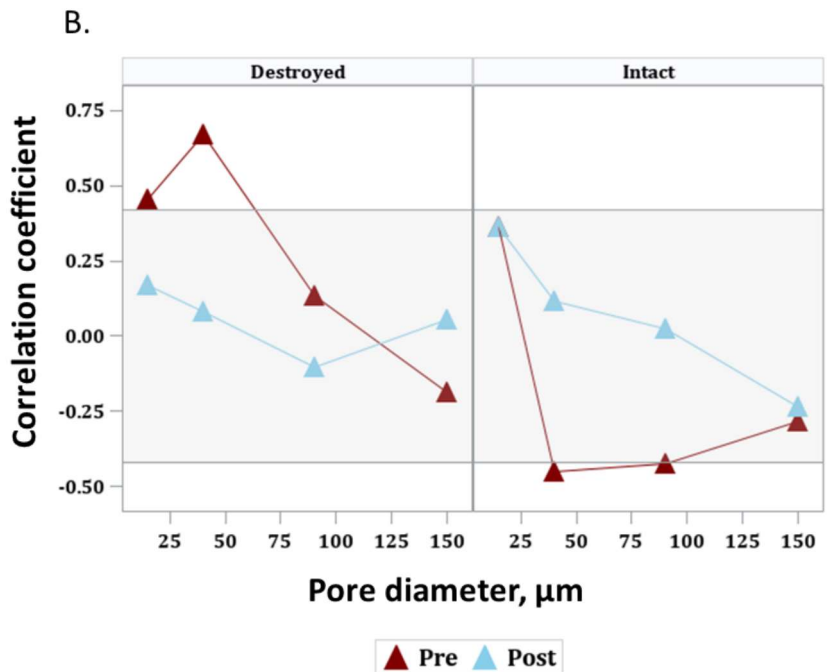
Figure 7: Color Please



**Figure 8**. Correlation coefficients between soil  $\delta^{13}$ C and relative abundances of 7-15 μm, 15-40 μm, 40-90 μm, and >90 μm Ø pores for the soil exposed to growing roots (**A**) and for the soil not exposed to roots (**B**) before (Pre) and after (Post) a 21-day incubation. Each correlation coefficient is based on the analysis of 15-25 observations. Examples of scatter plots and simple linear regression lines for the correlation coefficients reported in (**A**) are presented for destroyed and intact soil structures on Fig. 7 and Supplemental Fig.2, respectively. Gray area marks the range of correlation coefficient values that are not significantly different from zero at p<0.05 in data sets with 20 observations.

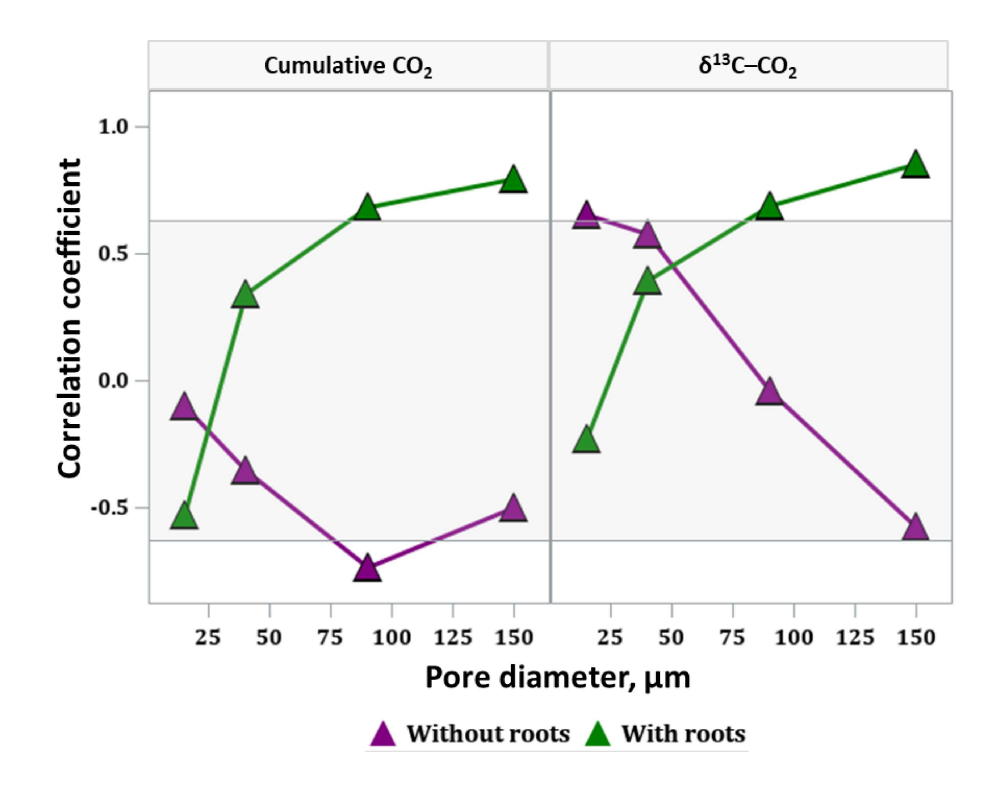
Figure 8: Color Please





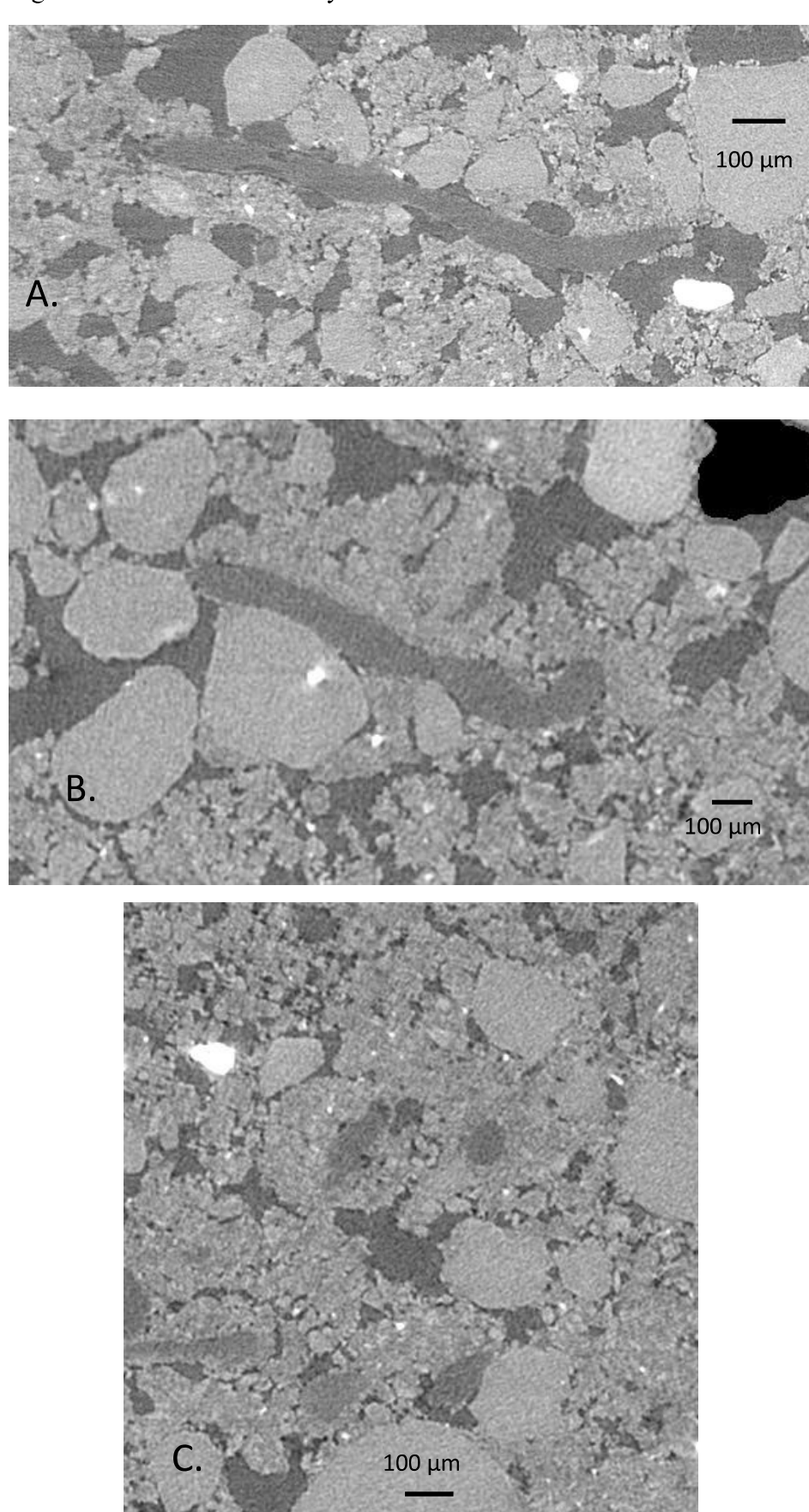
**Figure 9**. Correlation coefficients between cumulative  $CO_2$  emitted during a 21-day incubation and  $\delta^{13}C$  of the emitted  $CO_2$  with relative abundances of 7-15 μm, 15-40 μm, 40-90 μm, and >90 μm Ø pores for soil exposed and not exposed to growing roots. Each correlation coefficient is based on the analysis of 7-8 observations. Gray area marks the range of correlation coefficient values that are not significantly different from zero at p<0.05 for data sets with 8 observations.

Figure 9: Color Please.



**Figure 10**. Examples of roots creating new pores in sieved soil instead of following existing pore structure. A root cutting through existing pore structure (A). A root surrounded by soil as it grew past a sand grain (B). Several roots that grew down through soil where no larger pores seem to have existed prior to their growth (C).

Figure 10: No color necessary.



Conflict of Interest

**Declaration of interests** 

oxtimes The authors declare that they have no known competing financial interests or personal relationships that could have appeared to influence the work reported in this paper.
□The authors declare the following financial interests/personal relationships which may be considered as potential competing interests:

Supplementary Material

Click here to access/download **Supplementary Material**Supplemental Figures and Tables.docx